Multi-temporal InSAR analysis for monitoring ground deformation in Amorgos island, Greece

Stavroula Alatza[1], Ioannis Papoutsis[2], Demitris Paradissis[1], Charalampos Kontoes[2]

[1] National Technical University of Athens, School of Rural and Surveying Engineering , Higher Geodesy Laboratory and Dionysos Satellite Observatory, 9 Iroon Polytechniou str, 15780 Zographos, Greece, (ralatza@central.ntua.gr), (dempar@central.ntua.gr)

[2] National Observatory of Athens, Institute for Astronomy, Astrophysics, Space Applications & Remote Sensing, Vas. Pavlou & I. Metaxa str, 15236 Penteli, Greece, (ipapoutsis@noa.gr), (kontoes@noa.gr)

Key words: *SAR Interferometry; ground deformation; Amorgos earthquake; Sentinel-1; timeseries analysis; LOS decomposition*

ABSTRACT

Radar Interferometry is a widely used method, for estimating ground deformation, as it provides millimeter accuracy and at the same time, a wide spatial coverage of the study area. Persistent Scatterer Interferometry (PS) and Small Baseline Subset (SBAS), are two of the most prevalent methods, for time series analysis in SAR Interferometry. On 9 July 1956, one of the strongest earthquakes of the 20th century in the area of South Aegean, occurred in Amorgos, with a magnitude of Ms=7.4. The objective of this research is to map ground deformation in Amorgos island, using InSAR techniques. We conducted a multi-temporal analysis of all available data from 2003 to 2018, by exploiting historical ENVISAT SAR imagery, as well as the dense archive of Sentinel-1 SLC imagery. Results of both datasets indicate a small-scale deformation on the island. A multi-track analysis was implemented on Sentinel data, to decompose the line of sight velocities, to vertical and horizontal. The central south coast is experiencing horizontal movement, while uplift of a maximum value of 5mm/y, is observed in the southeastern coast. The combination of the good spatial coverage achievable via InSAR, with GPS measurements, is suggested as an important tool for the seamless monitoring of Amorgos island, towards tectonic hazard estimation.

I. INTRODUCTION

Greece is situated on the convergence limits, between the Eurasian and the African lithospheric plates, and therefore, is considered as one of the most seismogenic areas on the world. Amorgos is an island in South Aegean, which is situated NE of Santorini and NW of Astypalea islands (Figure 1). On 9 July 1956, a strong earthquake, with a magnitude of Ms=7.4, occurred in the Aegean Sea, 20 km south of Amorgos island.

The earthquake, induced a tsunami, probably caused by submarine sediment slumping, between Amorgos and Astypalea (Perissoratis et al., 1999). The damage caused by this earthquake was severe, in Amorgos, but also on the surrounding islands. The tsunami triggered by the earthquake, over the southern Aegean Sea, induced considerably more damage within a region of about 100 km. The seismic event caused the death of 53 people. 100 people were injured, 529 buildings were destroyed and more than 3200 buildings severely damaged.

In this paper, we present small-scale ground displacements, on Amorgos island, through geodetic observations of more than a decade.

We conducted a multi-temporal analysis of Synthetic Aperture Radar (SAR) imagery, from 2003 to 2018, using Persistent Scatterer Interferometry (PS) (Ferretti et al., 2001) and Small Baseline Subset (SBAS) (Berardino et al., 2002) techniques, to produce ground velocities maps for the island. A decomposition of the line of sight velocities to vertical and horizontal components was performed, combining measurements from ascending and descending imaging geometries for the 2014-2018 period and an estimation of vertical velocities for the 2003-2011 period.
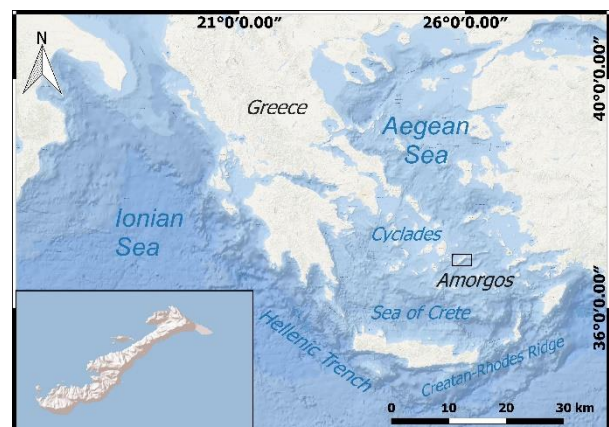

Figure 1. Location of the study area. Amorgos is depicted with the black rectangle. The inset image is a closer view of the island

II. TECTONIC SETTING

Amorgos belongs to the Cyclades island group, which lies to a very active tectonic zone, in the Aegean Sea

Plate (Figure 2). There exists morphotectonic evidence for long-term tilting of Amorgos, with uplift of the SE coast and subsidence of the NW coast, dominated by normal faulting (Papadopoulos and Pavlides, 1992; Rosenbaum and Ring, 2007), and this result is consistent with evidence of seismic uplift in the area of Hozoviotissa and drowning of ancient remains in the NE coast (Stiros et al., 1994). The destructive earthquake and tsunami of 1956, with an epicenter located between the Santorini-Amorgos graben, arose a great interest within the scientific community. The study of this seismic event and post-seismic deformation is of undoubted importance in our understanding of South Aegean seismotectonics.
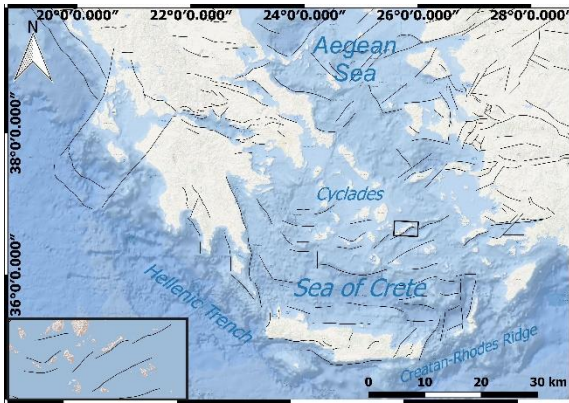

Figure 2. Fault sources in Greece as obtained by The European Database of Seismogenic Faults. Amorgos is depicted with the black rectangle. The inset image indicates the faults near Amorgos island

III. DATASETS AND PROCESSING

Timeseries analysis was performed on 24 ENVISAT SAR images from 2003 to 2011, and 106 Sentinel-1 images from 2014 to 2018. The datasets information is summarized in Table 1. Figure 3 presents the area of interest and the footprints of the satellite passes selected for Amorgos island. All scenes were provided by the European Space Agency (ESA). SNAP software (Sentinel Application Platform) (ESA, 2018b) was used for the processing of Sentinel-1 imagery. ROI_PAC software (Repeat Orbit Interferometry Package), by California Institute of Technology and Jet Propulsion Laboratory and DORIS (Delft object-oriented interferometric software), developed by the Delft Institute of Earth Observation and Space Systems, were used for the processing of ENVISAT SAR data. The multi-temporal interferometry (MTI) was performed with StaMPS/MTI (Stanford Method for Persistent Scatterers - Multi-Temporal InSAR) (Hooper et al., 2008), using PS and SBAS techniques, as well as the combination of the above methods.
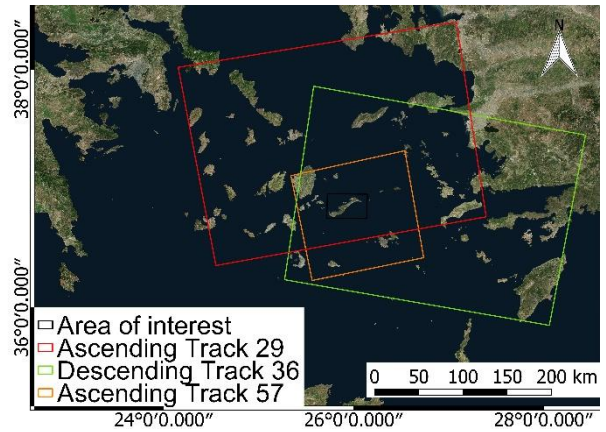

Figure 3. Map of the area of interest and the corresponding footprints of the satellite tracks of the datasets

Table 1. Data info

	SENSORS		
	ENVISAT SAR	SENTINEL	
Number of scenes	24	45	61
Relative orbit	57	36	29
Time interval	2003-2011	2014-2018	2014-2018
Swath type	I2	n/a	n/a
Sensor's Pass	Ascending	Descending	Ascending
SAR mode	n/a	IW	IW

A. The 2003-2011 period

Twenty-four raw ENVISAT SAR acquisitions of ascending track 57, were processed for the period 2003 to 2011. The lack of an adequate number of scenes, in the descending track 150, that covers the area of interest, led to the exclusion of this satellite pass from the estimation of ground displacements. Initially, we focused the raw data to Single Look Complex images, using ROI_PAC software. In order to improve the density of the coherent pixels, we oversampled the SLC images by a factor of two in azimuth and range direction (Sousa et al., 2011). We used the orbital data of the Department of Earth Observation and space systems (DEOS) of the Delft University of Technology and ESA. Differential interferograms were formed with DORIS software. For the estimation of the topography effect, we used the SRTM DEM (Farr et al., 2000).

For the PS analysis, a master image is selected to form N-1 interferograms with all the remaining scenes. The PS technique identifies pixels with stable backscattering characteristics, that are called persistent scatterers. In our study, the image that minimizes the temporal and perpendicular baselines is the scene of 4th July 2008. A baseline plot for the PS analysis, is shown in (Figure 4).
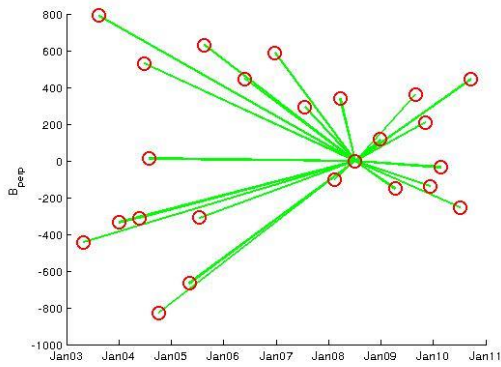
Figure 4. PS baseline plot for Envisat images-Ascending track 57

The SBAS technique, in StaMPS software, uses interferograms with the minimum Doppler, temporal and perpendicular baselines. The formation of a dense, uniform network of interferograms is important for the SBAS analysis, as shown in Figure 5.

The maximum uncorrelated DEM error and the phase noise standard deviation for all pixel pairs, are important parameters during the processing. To have a larger pixel sampling, considering the small interferometric stack, we selected a higher value of the default threshold (10m) for the maximum topographic error, which leads to a higher mean γ value (Hooper et al., 2007) of pixels that have random phase. The γ measure is a similar parameter to a measure of coherence (Bamler and Just, 1993). A lower value for standard deviation threshold, at a subsequent processing step, contributed to the elimination of noisy pixels and those selected due to signal contribution from neighboring ground resolution elements.
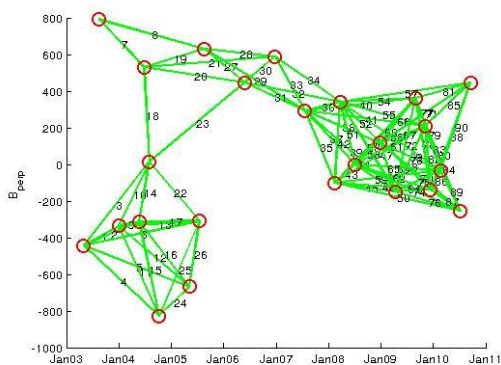

Figure 5. SBAS baseline plot for ENVISAT SAR data- Ascending Track 57

Additionally, the combined MTI processing was applied. During this step pixels selected by both PS and SBAS methods are combined before the phase unwrapping step. The advantage of this step is the mitigation of the phase unwrapping errors, leading to a

higher signal-to-noise ratio (SNR) and an improved spatial sampling.

B. *The 2014-2018 period*

The Copernicus program succeeded the Envisat mission, which ended on 8 April 2012. The Sentinel-1 mission consists of a constellation of two C-band sensors, Sentinel-1A (S-1A) and Sentinel-1B (S-1B). The short revisit time (6 days), offers a consistent long-term remote sensing data archive and provides a reliability on applications, requiring long time series. The Interferometric Wide (IW) swath mode, acquires data with a 250km swath, with high spatial resolution of 5x20m, and by using Terrain Observation with Progressive Scans SAR (TOPS) captures three sub-swaths in range-direction (De Zan et al., 2006). Each sub-swath is separated in nine bursts in azimuth direction.

For the 2014 to 2018 period, we performed Persistent Scatterer analysis on Sentinel-1 datasets of both ascending and descending tracks. 45 images of descending track 36 and 61 images of ascending track 29, were selected and processed.

The preprocessing of Sentinel-1 SLC images, as already mentioned, was performed in SNAP software. In order to achieve a less time-consuming process and meet the requirements of Sentinel datasets in computing storage and memory, we used SNAP's TOPSAR-Split operator, to select the swath and the number of bursts that cover Amorgos island. Orbital information was used, to gain accurate satellite position and velocity information.

Elevation Antenna Patterns correction was applied to Sentinel-1 acquisitions before March 2015, in order to compensate for the induced phase difference between the polarimetric channels.

Taking benefit of the high temporal and spatial resolution, provided by the Sentinel-1 data, we were able to select and include in the PS processing the interferometric pairs, characterized by small baselines and high estimated coherence rates.

The selection of the master image was based on the minimum temporal and perpendicular baseline thresholds. The 9th October 2016 scene provided the maximum estimated coherence for the interferometric stacking, of the descending track and the 20th October 2016 scene, for the ascending track (Figure 6).

All images are co-registered to the master image selected, using the back-geocoding operator. Before the interferogram formation, an additional processing of the bursts is necessary, due to the TOPS SAR mode characteristics. In Sentinel-1 TOPSAR, the imaged ground area of adjacent bursts will only marginally overlap in azimuth, therefore the deburst step is essential to solve pixel overlapping. Single master interferograms are formed, with subtraction of the flat-earth (reference) phase. The topographic phase was subtracted, using the SRTM DEM (Farr et al., 2000).

For the time-series analysis, we implemented the Stanford Method for Persistent Scatterers (Hooper et al., 2007), as described in the III.A. section, referring to the 2003-2011 Envisat period.
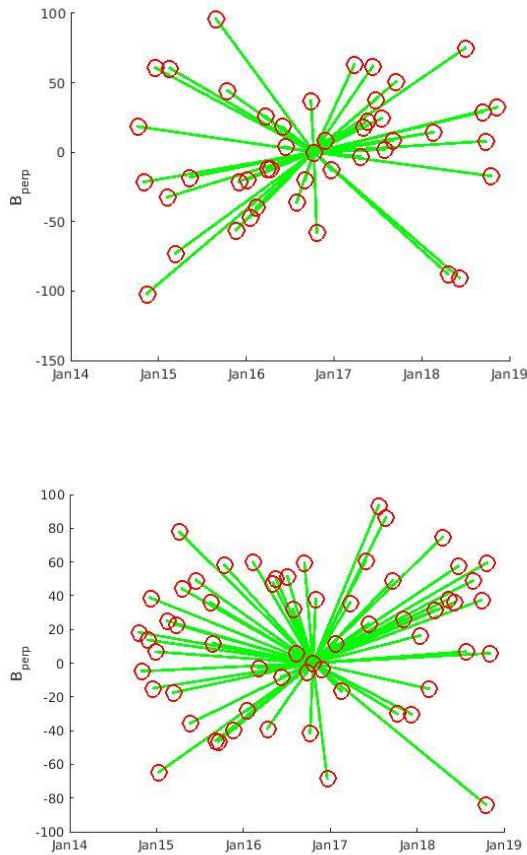

Figure 6: PS baseline plots of Sentinel-1 data- Upper: Descending track 36. Lower: Ascending track 29

IV. RESULTS

A residential area near Rachidi, that we expect to be quite stable in terms of deformation, was selected as a common reference area for both tracks. Line of Sight velocities relative to this reference area were estimated for all datasets. The results of the processing are shown in Figures 7, 10 and 11. Although, Persistent Scatterer Interferometry is very effective in analyzing deformation in urban areas, the StaMPS methodology, exploits spatial correlation of interferogram's phase to identify point targets in all terrains. In Amorgos case, where most of the island consists of pastures and only a 6% represents the residential area, the use of the StaMPS method, ensured the identification of persistent scatterers. The PS processing of Sentinel-1 data, resulted in 34393 scatterers for the ascending track and 49993 for the descending track. In all stacks from 2003 to 2018 the deformation rates are low and comply with the 1mm/y precision in PS measurements for linear deformation. The two islets Nikouria and Gramvoussa, were included in the InSAR analysis, assuming that from the coastline to the islets, the phase

difference between two samples, should be lower than π ($|\Delta\varphi| = |\varphi_i - \varphi_{i-1}| < \pi$).

A. The 2003-2011 period

The LOS displacements from 2003 to 2011 (Figure 7), indicate a small-scale displacement in most parts of the island and the two islets. Noticeable is the Hozoviotissa Monasterion region, that shows subsidence of 5mm/y, shown in Figure 8, in the timeseries plots generated for several scatterers within a region of 50 meters radius, around the Hozoviotissa region. Also, the south coast between Asfontilitis and Aegiali regions, is subsiding with a maximum velocity of 4mm/y (Figure 9). The southeastern coast of Amorgos is uplifted with a maximum velocity of 4mm/y.
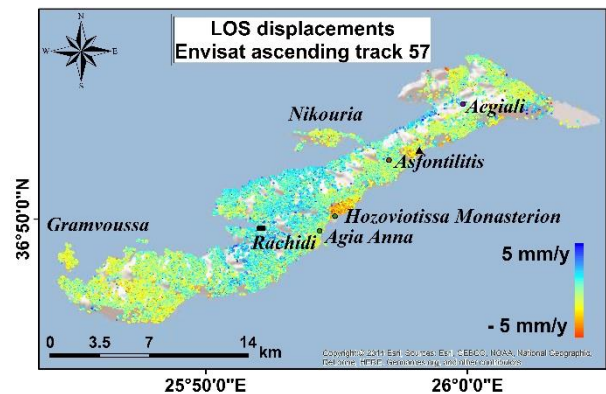

Figure 7. PS-SBAS combination LOS velocities of ENVISAT SAR images-Ascending track 57. The reference area near Rachidi is marked with the black rectangle. The black triangle represents the area between Asfontilitis and Aegiali regions
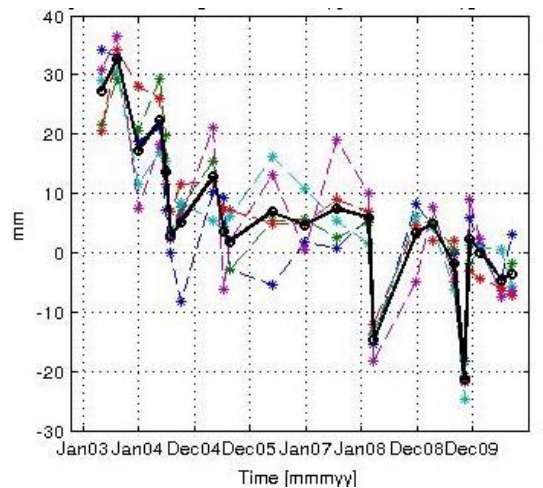

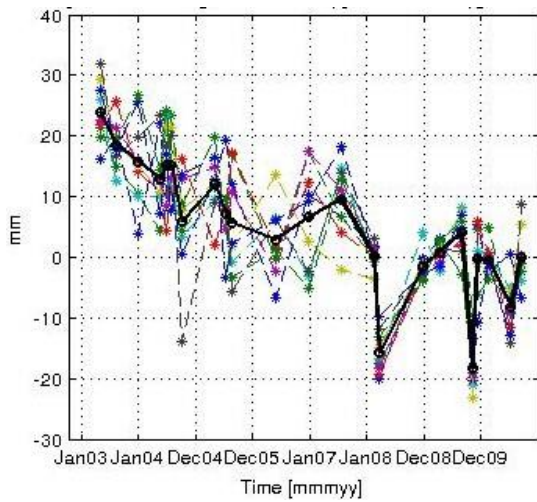Figure 8. Timeseries plot for Hozoviotissa Monasterion

Figure 9. Timeseries plot of the coast between Asfontilitis and Aegiali region

B. *The 2014-2018 period*

The LOS displacements estimated during this period (Figure 10) (Figure 11), comply with the deformation pattern estimated during the previous period (Figure 7). Low-rate velocities, not exceeding 2mm/y towards and away from the satellite, dominate in most parts of the island and the two islets. In the ascending track, the Hozoviotissa Monasterion coast is rather stable and the coast between Asfontilitis and Aegiali regions, is experiencing subsidence , but with lower velocity rates (4mm/y), as shown in the timeseries plot in Figure 12. While the results from both tracks for the majority of Amorgos agree, a significant difference is observed in the subsiding coasts of the ascending track. This shift in the direction of the deformation observed in the same coasts, for the descending track, is believed to be associated with horizontal movement contribution. In Sentinel-1 deformation maps, the southeastern part of the island, remains an uplifting area for both tracks, similarly to the 2003-2011 analysis, with a maximum velocity rate of 4mm/y.
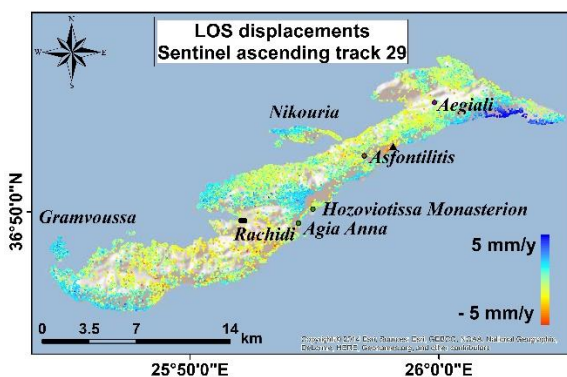

Figure 10. PS LOS velocities of Sentinel data for the ascending track 29. The reference area near Rachidi is marked with the black rectangle. The black triangle represents the area between Asfontilitis and Aegiali regions

Figure 11. PS LOS velocities of Sentinel data for the descending track 36 . The reference area near Rachidi is marked with the black rectangle. The black triangle represents the area between Asfontilitis and Aegiali regions
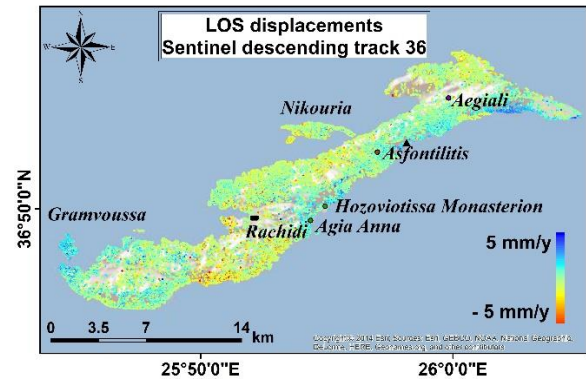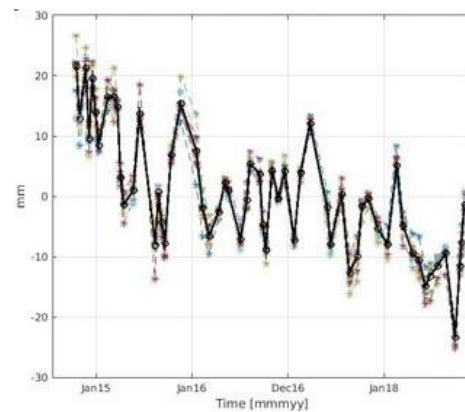

Figure 12. Timeseries plot for scatterers included in 50 meters radius, within the coast between Asfontilitis and Aegiali region, for the 2014-2018 period

C. *LOS displacements decomposition*

One limitation of InSAR is the difficulty in the interpretation of the earth's movements. SAR interferometry estimates velocities in the Line-Of-Sight direction. Therefore, displacements refer to a direction away from or towards the satellite. InSAR sensitivity is higher in the vertical component of the movement and minimal to the north component. This phenomenon is due to the near polar orbits and the small incidence angles of SAR satellites. The LOS velocities are the projection of 3D deformation on the line of sight direction (Equation 1). The Azimuth Look Direction (ALD) comprises information about the E-W and N-S motion components and is always perpendicular to the satellite heading. Figure 13 shows the geometry of the satellite's heading and Azimuth Look Direction (ALD) for the descending pass . We performed a decomposition of the LOS velocities, of the ascending (no.29) and descending (no.36) Sentinel-1 imaging geometries, to the vertical and horizontal components in the descending look direction.

$$v_{LOS} = v_{LOS_{Up}} + v_{LOS_{East}} + v_{LOS_{North}} \qquad (1)$$

The analysis is based on the hypothesis that a short distance between the PS scatterers, reflects a correlation in deformation. (Ketelaar et al., 2007). Following the methodology proposed by (Papoutsis et al., 2017), for ERS and ENVISAT sensors, initially we formed a grid that includes the area of interest. The dimensions are [25.74° 26.10°] in longitude and [36.76° 36.94°] in latitude, with a grid cell of 0.001° x 0.001° that correspond to an area of approximately 100x100m. The selection of the appropriate cell size depends on the distribution of the PS pixels and requires a balance between extremely averaging the deformation rates and adding too much information. For each track the incidence angles for every PS scatterer are estimated.

North ▲
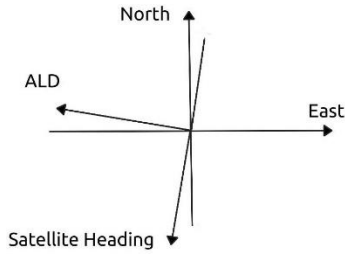
ALD

East

Satellite Heading ▼

Figure 13. Satellite's heading and Azimuth Look Direction for the descending pass

The shape of the island required a constant control of the patches, in every step of the analysis, in order to exclude those with zero PS scatterers. The centre of each cell is calculated, and a spline interpolation is used to estimate the look-angle of the centre from the corresponding values of the PS pixels included in each cell. Within each patch an averaging of the LOS velocities is performed. For the heading angle rates, we used an average value for all pixels, which is around 350° for the ascending track and 190° for the descending track. For decomposing the LOS velocities to vertical and horizontal displacements, the system of Equations (2) and (3) for the descending azimuth look angle direction, as proposed by (Samieie-Esfahany et al., 2009), was solved for every common scatterer.

$$\begin{bmatrix} d_{LOS}^{asc} \\ d_{LOS}^{desc} \end{bmatrix} = A \cdot \begin{bmatrix} d_{Up} \\ d_{ALD} \end{bmatrix} \qquad (2)$$

$$A = \begin{bmatrix} cos(\theta^{asc}) & \dfrac{sin(\theta^{asc})}{cos(\Delta\alpha)} \\ cos(\theta^{desc}) & sin(\theta^{desc}) \end{bmatrix} \qquad (3)$$

where d_{LOS}^{asc} = deformation along LOS for the ascending satellite pass
d_{LOS}^{desc} = deformation along LOS for the descending satellite pass
d_{Up} = vertical deformation

d_{ALD} = projection of horizontal deformation in the descending azimuth look direction
θ^{desc} = incident angle of the descending satellite pass
θ^{asc} = incident angle of the ascending satellite pass
$\Delta\alpha = \alpha_{asc} - \alpha_{desc}$ satellite heading difference between ascending and descending pass

Due to the limitation of one satellite pass for the Envisat data, an accurate comparison between the two periods is unfeasible. Though, we converted the LOS displacements from the 2003-2011 period, to vertical velocities using the Equation 4.

$$v_{Up} = \dfrac{v_{LOS}}{cos(\theta)} \qquad (4)$$

where for each scatterer v_{Up} = vertical velocity
θ = incident angle
v_{LOS} = line of sight velocity

Considering the 1mm/y precision of the PS LOS velocities for both tracks, we estimated the precision of the vertical and ALD components, using the Equations 5 and 6. For the error analysis we used a mean value of 33.84° and 37.94° of the incidence angle, for the ascending and descending track, respectively, as well as the mean heading values, already used in the decomposition analysis. The precision of the vertical velocities is 0.98 mm/y and 1.1 mm/y for the horizontal component. The estimated precisions lay within the 1mm/y accuracy level, for PSI processing. We also assume that horizontal velocities are mainly due to east-west motion, due to InSAR low sensitivity to the north component.

$$\sigma_{V_{Up}} = \sqrt{\left(\dfrac{\theta_{V_{Up}}}{\theta_{V_{asc}}}\right)^2 \sigma_{V_{asc}}{}^2 + \left(\dfrac{\theta_{V_{Up}}}{\theta_{V_{desc}}}\right)^2 \sigma_{V_{desc}}{}^2} \qquad (5)$$

$$\sigma_{V_{ALD}} = \sqrt{\left(\dfrac{\theta_{V_{ALD}}}{\theta_{V_{asc}}}\right)^2 \sigma_{V_{asc}}{}^2 + \left(\dfrac{\theta_{V_{ALD}}}{\theta_{V_{desc}}}\right)^2 \sigma_{V_{desc}}{}^2} \qquad (6)$$

where $\sigma_{V_{Up}}$ = precision of vertical velocities
$\sigma_{V_{ALD}}$ = precision of ALD velocities
$\sigma_{V_{asc}}$ = precision of LOS velocities of the ascending satellite pass
$\sigma_{V_{desc}}$ = precision of LOS velocities of the descending satellite pass

The decomposition to vertical and horizontal velocities, add some information about ground movements on the island. During both time periods, low rate displacements are observed in most parts of Amorgos. The two most significant observations will be mentioned. Horizontal motion in Hozoviotissa Monastery coast and uplift in the southeastern coast of

Amorgos. The LOS displacements in Hozoviotissa Monastery region, as mapped in Figure 10 and Figure 11, are opposite between the two different satellite passes, thus horizontal movement, is more likely to occur . ALD velocities at this region and in the coast between Asfontilitis and Aegiali, are positive, with a maximum value of 10mm/y, indicating a westward trend, that might be associated with strike-slip components, following the interpretation of the main structures on Amorgos island by (Papadopoulos and Pavlides, 1992). Another significant observation is the vertical displacements in the southeastern coast of Amorgos, with a maximum value of 5mm/y. According to (Papadopoulos and Pavlides, 1992) and (Stiros et al., 1994), the southeastern coast is characterized by high relief, normal faulting and uplift. Figure 14 presents the horizontal velocities for Sentinel-1 data and Figure 15 the vertical.
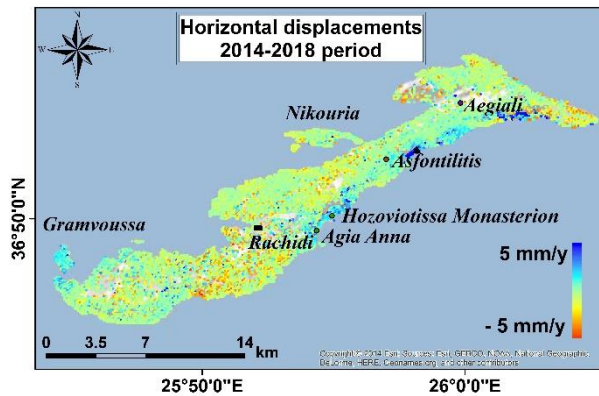

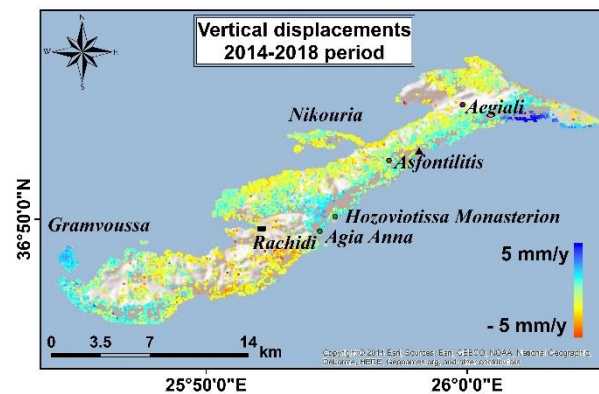Figure 14. Horizontal displacements for the 2014-2018 period

Figure 15. Vertical displacements for the 2014-2018 period

The vertical velocities for Envisat data are mapped in Figure 16. Although, the comparison between the two periods is unfeasible, we can obtain some information about the displacement field, from 2003 to 2011. We observe negative vertical velocities with a maximum value of -5mm/y in Hozoviotissa region and positive velocity rates of 4mm/y in the southeastern coast of Amorgos. The use of leveling data and GPS measurements, along with the InSAR results, could provide a better connection of these values with tectonic processes on the island.
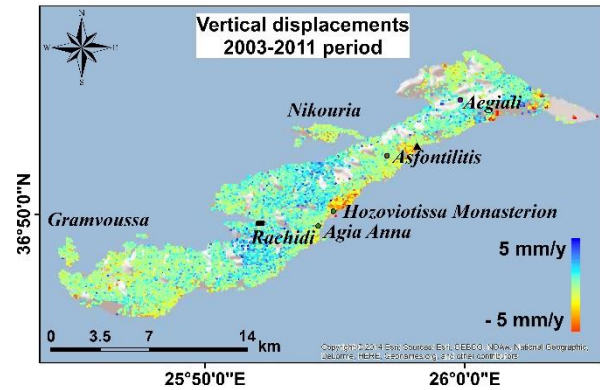

Figure 16. Vertical displacements for the 2003-2011 period for the ascending track 57

V. Conclusions

Time-series analysis of Envisat and Sentinel-1 satellite data was performed to study ground deformation in Amorgos island, from 2003 to 2018. Multi-temporal interferometry (MTI) using PS and SBAS techniques, as well as the combination of the above methods, was implemented in Envisat data. Line of sight velocities for Sentinel-1 images were estimated, using the PSI technique. For the 2014-2018 period, we combined observations from different imaging geometries to decompose the LOS velocities to horizontal and vertical components. Horizontal motion is observed in Hozoviotissa Monastery region. In addition, the southeastern coast of Amorgos, is uplifted. The estimation of vertical velocities for Envisat data, indicates subsidence in Hozoviotissa region and uplift on the southeastern coast of the island. In the absence of other geodetic observations, the 2003-2011 period, needs further investigation. Although, time-series analysis, is proved to be a very promising tool to monitor LOS displacements, a combination of SAR and GPS measurements on the island will increase the spatial as well as the temporal resolution and contribute to the validation of SAR displacements.

VI. Acknowledgements

References

Bamler, R., and D. Just, Phase statistics and decorrelation in SAR interferograms, Proc. Int. Geosci. Remote Sens. Symp., pp. 980 – 984, 1993

Berardino, P., Fornaro, G., Lanari, R. & Sansosti, E. (2002). A new algorithm for surface deformation monitoring based on small baseline differential SAR interferograms. IEEE Trans. Geosci. Remote Sens., 40 (11), pp. 2375–2383.

De Zan, F., & Guarnieri, A. M. (2006). TOPSAR: Terrain Observation by Progressive Scans. Geoscience and Remote

Sensing, IEEE Transactions on, 44(9), 2352-2360. doi:10.1109/TGRS.2006.873853

ESA, 2018a.Earth online. Missions. Sentinel-1

URL : https://earth.esa.int/web/guest/missions/esa-operational-eo-missions/sentinel-1

ESA, 2018b. Sentinel Application Platform v.7.0

URL : http://step.esa.int/main/toolboxes/snap/

Farr, T.G., Kobrick, M., Shuttle radar topography mission produces a wealth of data. Eos Trans. AGU 2000,81, 583-585.

Ferretti, A., Prati, C. & Rocca, F. (2001). Permanent scatterers in SAR interferometry. IEEE Trans. Geosci. Remote Sens., 39(1), pp. 8–20.

Hooper, A., P. Segall, and H. Zebker (2007), Persistent Scatterer InSAR for Crustal Deformation Analysis, with Application to Volcán Alcedo, Galápagos, J. Geophysical Research, 112, B07407.

Hooper, A. (2008). A multi-temporal InSAR method incorporating both persistent scatterer and small baseline approaches. Geophysical Research Letters, 35, L16302.

Ketelaar, G.; van Leijen, F.; Marinkovic, P.; Hanssen, R. Multi-track PS-InSAR datum connection. In Proceedings of the 2007 IEEE International Geoscience and Remote Sensing Symposium (IGARSS 2007), Barcelona, Spain, 23–28 July 2007; pp. 2481–2484.

Papadopoulos, G.A. And Pavlides, S.B. (1992) The large 1956 earthquake in the South Aegean: Macroseismic field configuration, faulting, and neotectonics of Amorgos Island, Earth and Planet. Sci. Lett. 113, 383-396. https://doi.org/10.1016/0012-821X(92)90140-Q

Papoutsis, I., C. Kontoes, D. Paradissis. (2017) Multi-Stack Persistent Scatterer Interferometry Analysis in Wider Athens,Greece, Remote Sensing 9 (3), 276, doi:10.3390/rs9030276

Perissoratis, C & Papadopoulos, Gerassimos. (1999). Sediment instability and slumping in the Southern Aegean Sea and the case history of the 1956 tsunami. Marine Geology. 161. 287-305. 10.1016/S0025-3227(99)00039-0

Rosenbaum, G. and Ring, U. 2007. Structure and metamorphism of Amorgos : a field excursion. In : (Eds.) Gordon S. Lister, M.A. Forster, and Uwe Ring, Inside the Aegean Metamorphic Core Complexes, Journal of the Virtual Explorer, Electronic Edition, ISSN 1441-8142, volume 27, paper 7, doi :10.3809/jvirtex.2007.00181

Samieie-Esfahany, S. ; Hanssen, R. ; van Thienen-Visser, K. ; Muntendam-Bos, A. On the effect of horizontal deformation on InSAR subsidence estimates. In Proceedings of the Workshop Fringe 2009, Frascati, Italy, 30 November–4 December 2009.

Sousa, J. J., A. Hooper, R. Hanssen, L. Bastos, and A. Ruiz, Persistent scatterer insar: A comparison of methodologies based on a model of temporal deformation vs. spatial correlation selection criteria, Remote Sensing of Environment, 115, 2652–2663, 2011.

Stiros, S., Marangou, L., and Arnold, M. : Quarternary uplift and tilting of Amorgos Island (southern Aegean) and the 1956 earthquake, Earth Planet. Sci. Lett., 128, 65–76, 1994.